Direct versus resonances mediated F+OH collisions on a new $^3A''$ potential energy surface

Susana Gómez-Carrasco
Departamento de Química Física, Facultad de Química, Universidad de Salamanca, 37008 Salamanca, Spain and Unidad Asociada UAM-CSIC, Departamento de Química Física, Facultad de Ciencias C-XIV, Universidad Autónoma de Madrid, 28049 Madrid, Spain

Lola González-Sánchez
Departamento de Química Física, Facultad de Química, Universidad de Salamanca, 37008 Salamanca, Spain and Unidad Asociada UAM-CSIC, Instituto de Matemáticas y Física Fundamental, CSIC, Serrano 123, 28006 Madrid, Spain

Alfredo Aguado
Unidad Asociada UAM-CSIC, Departamento de Química Física, Facultad de Ciencias C-XIV, Universidad Autónoma de Madrid, 28049 Madrid, Spain

Octavio Roncero
Unidad Asociada UAM-CSIC, Instituto de Matemáticas y Física Fundamental, CSIC, Serrano 123, 28006 Madrid, Spain

José M. Alvariño and M. Luz Hernández
Departamento de Química Física, Facultad de Química and Departamento de Física de la Atmósfera, Facultad de Ciencias, Universidad de Salamanca, 37008 Salamanca, Spain

Miguel Paniagua
Unidad Asociada UAM-CSIC, Departamento de Química Física, Facultad de Ciencias C-XIV, Universidad Autónoma de Madrid, 28049 Madrid, Spain

(Received 7 May 2004; accepted 16 June 2004)

A theoretical study of the $F(^2P)+OH(^2\Pi)\rightarrow HF(^1\Sigma^+)+O(^3P)$ reactive collisions is carried out on a new global potential energy surface (PES) of the ground $^3A''$ adiabatic electronic state. The *ab initio* calculations are based on multireference configuration interaction calculations, using the aug-cc-pVTZ extended basis sets of Dunning *et al*. A functional representation of the PES shows no nominal barrier to reaction, contrary to previous results by others. Wave packet and quasiclassical trajectory calculations have been performed for this PES to study the $F+OH(v=0,j)$ reactive collision. The comparison was performed at fixed and constant values of the total angular momentum from 0 to 110 and relative translational energy up to 0.8 eV. The reaction presents a dynamical barrier, essentially due to the zero-point energy for the bending vibration near the saddle point. This determines two different reaction mechanisms. At energies higher than ≈0.125 eV the reaction is direct, while below that value it is indirect and mediated by heavy-light-heavy resonances. Such resonances, also found in the simulations of the photodetachment spectrum of the triatomic anion, manifest themselves in the quasiclassical simulations, too, where they are associated to periodic orbits. © *2004 American Institute of Physics.* [DOI: 10.1063/1.1780168]

I. INTRODUCTION

The natural, atmospheric abundance of O-containing molecules makes reactions of atomic oxygen very important.[1] In the troposphere, this mainly applies to ground state oxygen $O(^3P)$,[2] while the first electronically excited state species $O(^1D)$ is of greater concern in the stratosphere where molecules (including ozone) easily dissociate under the action of solar UV radiation.

Metastable species such as singlet oxygen $O(^1D)$ are particularly active reagents, and its reaction with targets such as HCl or HBr (see Ref. 3 for a short review) has been much studied. These studies were based mainly on electronically adiabatic ground potential energy surfaces (PES) and quasiclassical trajectory (QCT) calculations. The quintuple degeneracy of the atomic reagent and the implied fivefold PES were ignored, as was the role of their mutual coupling. However, nonadiabaticity is more frequent than was previously thought in the behavior of molecular systems[4] and this should be specially the case whenever electronically excited atoms or molecules are in play.

Turning to $O(^3P)$ and because of the many similarities with this work, we notice a most recent *ab initio* calculation by Ramachandran and Peterson[5] for the closely related $O(^3P)+HCl(^1\Sigma^+)$ system. They obtained highly correlated and precise results for the $^3A''$ PES and $^3A'$ PES with a double objective: to account for an apparently anomalous trend of the experimental $k(T)$ at high temperatures (over 2000 K) and to improve the behavior of a previous, already very precise PES[6] by correcting (narrowing) the barrier shape to reduce the tunneling through it and (what very spe-

cially concerns our work as reported in this paper) to include for the first time the excited $^3A'$ PES in the calculations. The used level of theory and basis sets, the details of the obtained ground PES (specially the location, energy, and shape of the found van der Waals wells), in Ref. 5 and, as related quantum dynamics computations regards[7] (performed on the PES of Ref. 6), the finding of sharp resonances and their assignment to van der Waals quasibound states, all this is most relevant to results and findings of the present work as it will be opportunely pointed out.

Compared to the higher members of the family, OHF is a much less studied system both experimentally and theoretically. So, the

$$F(^2P)+OH(^2\Pi)\rightarrow O(^3P)+HF(^1\Sigma^+) \quad (1)$$

reaction, the reverse of $O(^3P)+HCl(^1\Sigma^+)$ taken in the exoergic sense, has been the subject of just a couple of kinetic flow experiments[8,9] Walther and Wagner[8] obtained a very small activation energy ($E_a=180$ K, less than 0.02 eV) compatible with the expected absence of potential energy barrier (E_b) on a very exoergic reaction, while, trying to lend support to their experimental results, Sloan and co-workers[9] did some *ab initio* calculations, exploring only collinear geometries. They found out for their lowest $^3\Pi$ surface a barrier height of 0.52 eV at $r_{OH}=1.08$ Å and $r_{HF}=1.32$ Å; their calculated reaction exoergicity, 1.198 eV, is much lower than the experimental one, 1.502 eV. Recently, both sets of experimental results were well simulated by QCT calculations[10] in the PES presented in this work.

There is a spectroscopy experiment of Neumark and co-workers,[11] closely related to reaction (1). In their experiment, Neumark *et al.* measured the kinetic energy spectrum of electrons photodetached by 213 nm UV photons from a diluted OHF^- gas. The process can be represented as

$$OHF^-(^2\Pi)+h\nu\rightarrow OHF+e^- \quad (2)$$

yielding the neutral unstable OHF intermediate in several electronic states and in the neighborhood of the transition state of reaction (1). The photoelectron spectrum, in fact, reflects features of the transition state region of the PES of the neutral.

To interpret their spectrum in terms of potential energy features, Neumark *et al.* calculated *ab initio* some properties of $OHF^-(^2\Pi)$. They used them together with the corresponding *ab initio* calculations for the neutral by Sloan and co-workers[9] to perform a wave packet propagation calculation at collinear geometries and to simulate the photoelectron experiment. Although the general trend was fairly good, several failures were noticed. Bradforth *et al.*[11] attributed this to a defect of the potential energy surface for the ground neutral reaction (1): E_b should lie, they argued, somewhere in the interval 0.09–0.40 eV, instead of the 0.52 eV of Ref. 9 and the barrier should be located earlier in the reactant valley.

Later on, Dixon and Tachikawa[12] calculated, at the MP4 level of perturbation theory, points for the ground $^3A''$ PES again mainly in the collinear configuration. Although an improvement in the agreement between theory and experiment was achieved, a fully three-dimensional PES and a calculation of excited states as was demanded by the authors of Ref. 11 continued to be necessary.

A recent three-dimensional simulation[13] of the photodetachment spectrum using the PES presented in this work yielded an even better agreement. These calculations showed narrow peaks associated to heavy-light-heavy (HLH) resonances, which were absent in the previous simulations. The remaining discrepancies were attributed to the contributions of other electronic states and this is the subject of a further work.[14]

Notwithstanding the success of QCT calculations,[10] the HLH mass feature of OH producing processes in which a light atom is exchanged between two heavy ones, and the expected hydrogen-bonded nature of the intermediates lets expect many exciting quantum features in OHX systems unadvertized by classical dynamics calculations. In order to include all the above-mentioned effects a detailed quantum treatment on the F+OH reactive collision is necessary. The difficulties of using quantum methods to treat such reactions have been recently reviewed.[15] The O+HX reactions and their reverse X+OH, feature three different atoms, wells (van der Waals but also chemical wells) and, in some cases, large exoergicities, and, therefore, present interesting difficulties for quantum simulations.

Having advanced some *ab initio* results as well as the simulation with QCT techniques of the available kinetic experimental data[10] this paper is devoted to a full description of highly accurate *ab initio* calculations for states connecting the $O(^3P)+HF(^1\Sigma^+)$ to the $OH(^2\Pi)+F(^2P)$ asymptotes, making emphasis on the $^3A''$ ground electronic state. The reaction dynamics is studied using wave packets and QCT methods with special attention being paid to the resonance structure of the quantum results and its classical counterpart. We close with some conclusions and prospectives.

II. *AB INITIO* CALCULATIONS AND FIT OF THE SURFACE

This paper focuses on the ground state $^3A''$ of OHF that adiabatically correlates with $F(^2P)+OH(^2\Pi)$, $O(^3P)+HF(^1\Sigma^+)$, and $H(^2S)+FO(^2\Pi)$ atom-diatom dissociation limits. In Fig. 1 we show qualitatively the correlation diagram for the lowest electronic states of interest. The $F(^2P)+OH(^2\Pi)$ reactants asymptotic limit correlates with singlet and triplet states of symmetry Σ^+, Σ^-, Π, and Δ in the $C_{\infty v}$ group (or three A' and three A'' in C_s). Among all of them, the $^3\Pi$ and $^3\Sigma^-$ states correlate with the ground states of products $O(^3P)+HF(^1\Sigma^+)$, while the $^1\Sigma^+$, $^1\Pi$ and $^1\Delta$ states correlate with the first excitations of products, $O(^1D)+HF(^1\Sigma^+)$.

The basis sets used in the present work are the correlation-consistent polarized valence triple zeta basis sets of Dunning and co-workers[16,17] augmented with diffuse functions for F, O, and H atoms, denoted aug-cc-pVTZ or AVTZ. These extra diffuse functions were optimized to reproduce the lowest state of the anion. In order to estimate the effect of higher angular momentum functions in the PES, some calculations have been performed with the more ex-

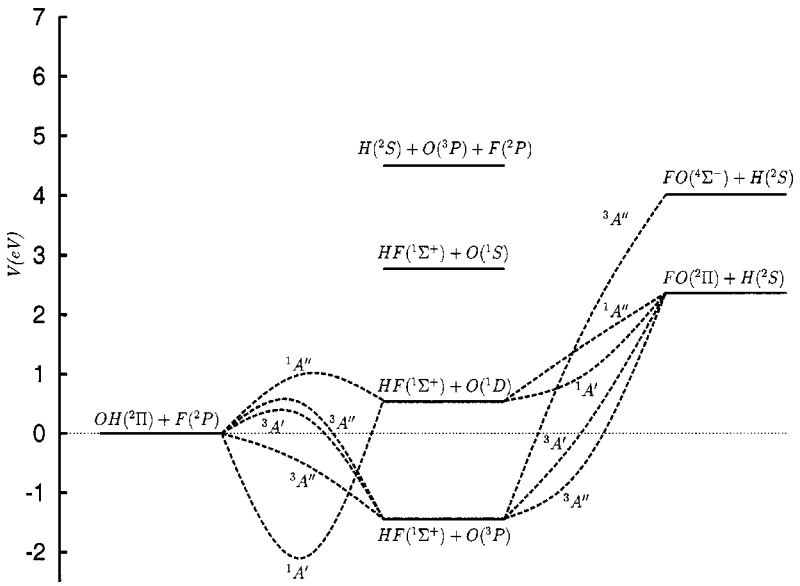

FIG. 1. Qualitative correlation diagram for the OHF system.

tended basis sets of Dunning *et al.* aug-cc-pVnZ or AVnZ, with $n=4$ and 5 (for quadruple and quintuple zeta, respectively).

All *ab initio* electronic structure calculations were carried out with the MOLPRO suite of programs.[18] As a starting point, a full valence state averaged complete active space calculation (SA-CASSCF) (Refs. 19 and 20) was performed. This includes all molecular orbitals arising from the valence atomic orbitals (14 electrons in 9 orbitals) what, with the AVTZ basis set (115 contracted Gaussian functions), includes 308 configuration state functions (CSFs) for the $^3A''$ symmetry. All calculations were performed in C_s symmetry. The two lowest a' CASSCF molecular orbitals (approximately, 1*s* orbitals on fluorine and oxygen atoms) have been optimized, but maintaining them doubly occupied. The number of states included in the SA-CASSCF calculation has been selected from the products asymptotic limits $O(^3P,^1D)+HF(^1\Sigma^+)$, i.e., three $^1A'$, two $^1A''$, one $^3A'$, and two $^3A''$. Thus, at collinear geometries the A' and A'' states, correlating to the Π or Δ doublets, become degenerate.

Internally contracted multireference configuration interaction (icMRCI) calculations,[21,22] with single and double excitations, have been done, using the CSFs obtained from the SA-CASSCF calculations as reference functions. Several tests have been performed with different SA-CASSCF functions, but the icMRCI calculations yield practically the same results. Finally, the Davidson correction (+Q) (Ref. 23) was applied to the final energies in order to approximately account for unlinked cluster effects of higher excitations. In this case, preliminary calculations of the two-degenerate states of Π symmetry (or Δ) show a small difference of about 0.1 m E_h (ca. 3 meV). The accuracy of the *ab initio* computations at the dissociation asymptotes can be assessed by comparing some calculated equilibrium spectroscopic data with experimental values for the OH, HF, and FO diatoms. For the reactants (OH+F) and products (HF+O) the diatomic potentials were computed placing the third atom about $20\,a_0$ away from the diatom. The icMRCI+Q calculations for the diatomics shown in Table I, are in rather good agreement with the experimental values. The dissociation energies D_0's of the three molecules are smaller than the experimental ones by about 0.2 eV. However, the agreement improves as the *AVnZ* basis set grows,[24] finally reaching a good accord with the experiment, specially for OH and HF.

A. Triatomic *ab initio* calculations

The attention of the work focuses on the ground triplet state $^3A''$, which, as shown in Fig. 1, correlates with the atom+diatom reactants' and products' ground states as follows:

$$F(^2P)+OH(^2\Pi)\rightarrow\begin{cases}O(^3P)+HF(^1\Sigma^+)\\H(^2S)+FO(^2\Pi)\,.\end{cases}$$

Several other (singlet and triplet) states have also been calculated but their discussion will be delayed for another work.

Ab initio calculations have been performed over an initial grid in the internal coordinates r_{HF}, r_{OH}, and OHF bond angle. The general grid is as follows:

TABLE I. Ground-states properties of HF, OH, and FO. A comparison between the fitted, calculated (icMRCI+Q) and experimental (Expt.) data.

Diatom		$HF(X^1\Sigma^+)$	$OH(X^2\Pi)$	$FO(X^2\Pi)$
r_e (Å)	Fit	0.9166	0.9735	1.3536
	icMRCI+Q	0.9165	0.9737	1.3642
	Expt.	0.9168[a]	0.9697[a]	1.3541[b,c]
ω_e (cm^{-1})	Fit	4170	3723	1071
	icMRCI+Q	4154	3723	1039
	Expt.	4138[a]	3738[a]	1053[b]
D_0 (eV)	Fit	5.685	4.270	2.070
	icMRCI+Q	5.685	4.270	2.067
	Expt.	5.869[a]	4.392[a],4.415[d]	2.235[e]

[a]Reference 26.
[b]Reference 56.
[c]Reference 57.
[d]Reference 27.
[e]Reference 58. The error bar of D_0 for FO is ± 0.098 eV.

TABLE II. icMRCI+Q geometry and energy of stationary points calculated with several basis sets and extrapolated CBS energies. Energies in eV and distances in Å.

Point	r_{OH}	r_{HF}	θ	Energy
		aVTZ		
Reactants	0.9737	⋯	⋯	0.000
Products	⋯	0.9165	⋯	−1.443
Minimum $M1$	0.9822	2.0924	66.4	−0.230
Minimum $M2$	1.9214	0.9308	180.0	−1.589
Transition state	1.0330	1.3494	109.2	−0.002
		aVQZ		
Reactants	0.9710	⋯	⋯	0.000
Products	⋯	0.9224	⋯	−1.432
Minimum $M1$	0.9742	2.0881	66.3	−0.227
Minimum $M2$	1.9146	0.9276	180.0	−1.584
Transition state	1.0324	1.3420	109.2	0.007
		aV5Z		
Reactants	0.9705	⋯	⋯	0.000
Products	⋯	0.9218	⋯	−1.427
Minimum $M1$	0.9737	2.0892	66.3	−0.221
Minimum $M2$	1.9204	0.9271	180.0	−1.574
Transition state	1.0324	1.3399	109.3	0.017
		CBS		
Reactants	⋯	⋯	⋯	0.000
Products	⋯	⋯	⋯	−1.424
Minimum $M1$	⋯	⋯	⋯	−0.218
Minimum $M2$	⋯	⋯	⋯	−1.568
Transition state	⋯	⋯	⋯	0.022

$$r_{HF}=1.2-7.0a_0 \quad (25 \text{ values}),$$

$$r_{OH}=1.3-7.2a_0 \quad (25 \text{ values}),$$

$$\theta(\mathrm{OHF})=0-180^\circ \quad (10 \text{ values}),$$

corresponding $\theta=180°$ to collinear OHF and $\theta=0°$ to both collinear HOF and OFH structures. Moreover, in order to obtain an accurate fit for the minimum energy path (MEP) and the energetically low lying regions, we have computed additional points along a MEP, obtained using preliminary fits to the general grid. Additional points have been selected in order to take into account all the asymptotic channels shown in Fig. 1 up to 4.5 eV with respect to the zero of energy, located at the reactants F+OH asymptote, the origin of energy hereafter used in this work. All in all 8069 points were used to fit the final ground potential energy surface, as described below.

Geometries of the stationary points as well as of the reactant and product channels have been optimized with the AVnZ (with $n=3$, 4, and 5) extended basis sets of Dunning *et al.* The inclusion of higher angular momentum functions in the basis sets shows that the AVTZ basis provides results accurate enough, as can be seen in Table II, where the computed relative energies and optimized geometries are compared. The energy difference between the AVTZ and AV5Z results is only about 0.01 eV, and the geometry difference is, in general, lower than 0.01 Å for the distances or 0.1° for the OHF angle. Note that the icMRC+Q calculations with the AVQZ and AV5Z basis sets (with 206 and 334 contracted functions, respectively) involve a number of contracted (uncontracted) configurations of the order of 1 000 000 (82 000 000) and 2 500 000 (225 000 000), respectively, making the calculation of the whole surface with these basis sets computationally too expensive.

In view of the regular variation with n of the stationary energy values calculated with the different AVnZ ($n=3$, 4, and 5) basis sets, we used the expression[25]

$$E(n)=E_{CBS}+Be^{-(n-1)}+Ce^{-(n-1)^2}$$

to calculate E_{CBS}, the extrapolated infinity ($n=\infty$) basis-set limit energy. As seen in the last column of Table II, the energy differences between the CBS and AVTZ stationary points values do not exceed 20 meV, thus showing the accuracy of the AVTZ results used in this work.

Finally, the calculated exoergicity for the reaction $F(^2P)+OH(^2\Pi)\rightarrow O(^3P)+HF(^1\Sigma^+)$, obtained from the energy dissociation for the diatoms, is 1.416 eV, including the harmonic zero point energies (ZPE). The experimental exoergicity, 1.477 or 1.454 eV, corresponding to the two experimental results for OH (Refs. 26 and 27) (see Table I), is in good agreement with the calculated one, better than 4%. Note that the experimental values contain contributions from spin–orbit coupling in O(≈0.010 eV), F(≈0.017 eV) and OH(≈0.005 eV), that are not included in the *ab initio* calculations. This spin–orbit contribution would make the agreement with the experimental one slightly worse (≈0.012 eV).

B. Global potential energy surface

The calculated icMRCI+Q energies for the ground $^3A''$ electronic state have been fitted using the procedure developed in Refs. 28 and 29. The PES is represented by a many-body expansion,

$$V_{OHF}=\sum_{A}^{3} V_A+\sum_{AB}^{3} V_{AB}^{(3)}(r_{AB})+V_{ABC}^{(3)}(r_{AB},r_{AC},r_{BC})$$

Each two-body potential is written as a sum of short- and long-range terms, $V_{AB}^{(2)}=V_{short}+V_{long}$, with

$$V_{short}=c_0\frac{e^{-\alpha r_{AB}}}{r_{AB}} \quad (c_0,\alpha>0)$$

$$V_{long}=\sum_{i}^{L} c_i\rho_{AB}^{i},$$

$$\rho_{AB}(r_{AB})=r_{AB}e^{-\beta_{AB}^{(N)}r_{AB}} \quad (\beta_{AB}>0),$$

where the c_i $(i=0,...,L)$ are linear fitting parameters, and α and $\beta_{AB}^{(N)}$ (with $N=2$) are nonlinear fitting parameters. The variables ρ_{AB} are modified Rydberg functions that depend on the internuclear distances and tend to zero when the corresponding distance goes to zero or to infinity. The term V_{short} takes into account the repulsive part of the potential, and goes to infinity when $r_{AB}\rightarrow 0$. The root-mean-square errors (rms) of the fitted potentials from *ab initio* values are 1.6, 2.2, and 6.1 meV for OH, HF, and FO, respectively. Note that the FO diatom is energetically not accessible in the energy range of interest, see Fig. 1. The agreement of the basic spectroscopic constants of the electronic ground states for the three diatomics is shown in Table I, where we compare the

fitted, *ab initio* and experimental data. Since these quantities are very sensitive to the shape of the potential near the minimum, in order to obtain a better agreement between the fitted and calculated frequencies, it is necessary to use a greater number of *ab initio* points. This is the case for the FO diatom, but is not too important because it is a closed channel in the energy range of interest.

The three-body term is expressed as the expansion,

$$V_{ABC}^{(3)}(r_{AB},r_{AC},r_{BC})=\sum_{ijk}^{K} d_{ijk}\rho_{AB}^{i}\rho_{AC}^{j}\rho_{BC}^{k}$$

in the same type of Rydberg functions as above with $N=3$. The linear parameters d_{ijk} $(i+j+k\leqslant K)$ and the three nonlinear parameters $\beta_{AB}^{(3)}$, $\beta_{AC}^{(3)}$, and $\beta_{BC}^{(3)}$ are determined by fitting to the last equation the 8069 calculated *ab initio* energies after substraction of the total two-body contributions. The overall root-mean-square errors of the fitted PES is 0.043 eV and the maximum error ($E_{\max}$) amounts to 0.41 eV and it is located in a repulsive region, as shown in Table III. The energy range of the fitted PES goes from -1.58 eV up to values over the three atom (H+F+O) dissociation limit (4.5 eV), an unusually large range. In addition we point out the problems of fitting an adiabatic ground $^3A''$ PES featuring several intersections with the excited states, an issue to be dealt with elsewhere.[14]

In order to have a more detailed view of the accuracy of the fitted PES, we also report in Table III the rms errors and maximum deviations subdivided in several energy regions: the O···HF van der Waals (vdW) well of the products region is below -1.20 eV, and the saddle point and the F···OH vdW well in the reactants channel are in the -0.24 to 0.24 eV interval. There are $\Sigma^{-}-\Pi$ vibronic intersections in the interval -1.20 to -0.24 eV, that makes the rms error in this interval slightly worse. In the lower part of Table III, the rms errors and $E_{\max}$ values are shown, ordered following a geometrical criterion, namely, long, intermediate, and short distances regions, as well as according to the different chemical arrangements.

TABLE III. Root mean square (rms) and maximum deviation ($E_{\max}$) in eV of the *ab initio* data from the fitted ones for several energy and geometry ranges, for the $X\,^3A''$ state of OHF. N is the number of *ab initio* points in every energy range.

	N	rms	$E_{\max}$
Energy range			
$E>0.24$	3331	0.057	0.41
$-0.24<E<0.24$	1897	0.029	0.19
$-1.20<E<-0.24$	833	0.044	0.25
$E<-1.20$	2008	0.019	0.14
All data points	8069	0.043	0.41
Geometry range			
Long distances	411	0.018	0.08
Intermediate distances	2369	0.044	0.32
Short distances	782	0.078	0.41
OH channel	1753	0.037	0.29
HF channel	2433	0.027	0.22
OF channel	321	0.030	0.19

C. Topological characteristics

The main topological characteristics of the OHF $^3A''$ PES are shown in the MEP displayed in Fig. 2. It was obtained following the gradient extremal path[30,31] as a function of the arc length s, defined as the sum of the displacements ds between two consecutive points of the surface in terms of the three internuclear distances.[31] By convention, we take ds positive from the saddle point toward products (O+HF) and negative toward reactants (OH+F). As shown in the MEP, there are two rather deep hydrogen-bonded wells, located in the reactants and products regions, and a saddle point between them: this is, actually, the transition state (TS) for reaction (1).

In Table IV we present the geometries and energies of the stationary points of the fitted $^3A''$ PES and a comparison with the *ab initio* icMRCI+Q values. The F···OH vdW reactants well (minimum M1) is located at an angle of 59.7° at 0.230 eV while the O···HF vdW products well (minimum $M2$) has a collinear configuration and an energy of 1.587 eV below the reactants asymptote. A normal mode analysis has been performed both for the analytical fit as well as from the *ab initio* calculations in the neighborhood of the energy minima. All calculated frequencies for both vdW complexes have real values, indicating that they are minima of the fitted PES. Moreover, to assess the accuracy of the fitted PES, both *ab initio* and fitted harmonic normal modes are shown in Table IV. They are denoted as (v,n,b), and on examination it turns out that they can be described as approximately corresponding to OH(v) and HF(n) stretching and O—H—F(b) bending. The OH vibration frequency ($\omega_v \approx 3600\,\mathrm{cm}^{-1}$) for the $M1$ minimum is slightly lower than that of free OH ($\omega\approx 3720\,\mathrm{cm}^{-1}$). For the other minimum $M2$ the highest frequency corresponds to the HF vibration ($\omega_n \approx 3800-4000\,\mathrm{cm}^{-1}$), being something lower than that of free HF ($\omega\approx 4150\,\mathrm{cm}^{-1}$). At this collinear equilibrium geometry, the bending mode is, of course, doubly degenerate, with $\omega_b\approx 350\,\mathrm{cm}^{-1}$. We point out that two very similar (geometries, energetics, and even harmonic frequencies) van der Waals wells have been found by Ramachandran and Peterson[5] in an analogous *ab initio* study of the PES for the $O(^3P)+HCl(^1\Sigma^+)$ reaction.

As expected for an exoergic reaction[32] the transition state (TS) is an early one, i.e., it is placed in the reactants channel. It lies at a r_{OH} distance slightly elongated with respect to the free OH equilibrium distance, and at an OHF angle $\theta=109.6°$. The normal mode associated to the imaginary frequency, $\omega_n\approx 1420i\,\mathrm{cm}^{-1}$, corresponds to the HF displacement, whereas the frequency associated to the OH vibration, $\omega_v\approx 2550-2650\,\mathrm{cm}^{-1}$, is much lower than that of free OH. This transition state is located at an energy of 7 meV above the reactants asymptote, showing that this reaction has practically no nominal barrier. As a further proof of the quality of the fit, these results are in very good agreement with the *ab initio* ones as shown in Table IV (and in Table II with several basis sets), being the energy difference of about 0.01 eV. Also, Table IV shows the harmonic vibrational frequencies of the transition state for both the *ab initio* icMRCI+Q and fitted PES. The inclusion of the harmonic ZPE into the reactants (0.231 eV) and into the transition state (0.178 eV) structures gives an effective ''barrier'' to reaction

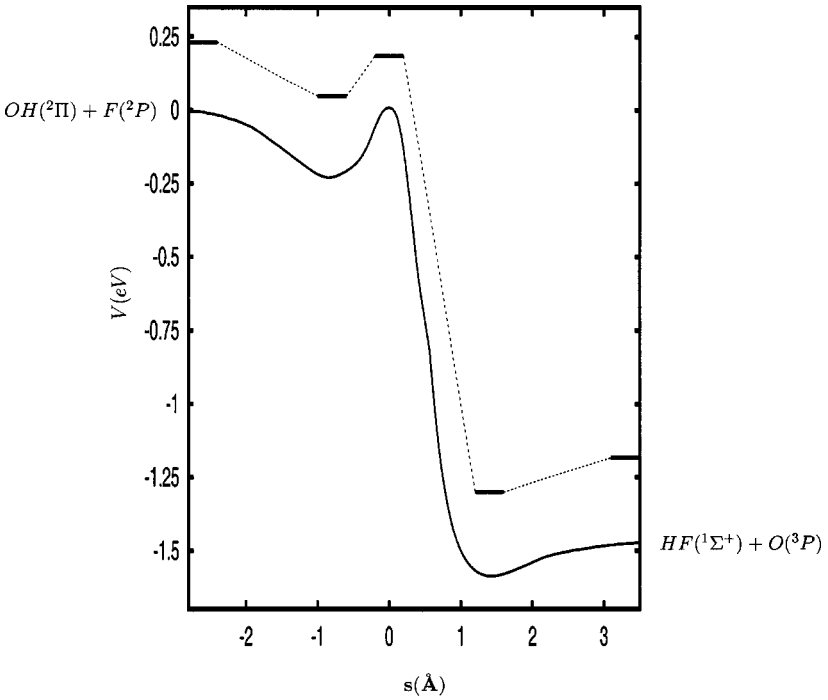

FIG. 2. Minimum energy path of the three-dimensional $^3A''$ ground state PES for the $F(^2P)+OH(^2\Pi) \rightarrow O(^3P)+HF(^1\Sigma^+)$ reaction. Dotted lines connect the stationary points including the zero-point energy.

of -0.046 eV, i.e., there is no energy threshold to reaction, as shown in Fig. 2.

In Fig. 3 contour plots for three cuts to the fitted $^3A''$ PES are shown, corresponding the upper panel to the bent saddle point ($\theta=109.6°$), the middle panel to the van der Waals reactants well ($\theta=59.7°$), and the bottom panel to the van der Waals products well ($\theta=180°$), respectively.

It is also interesting to show the angular dependence of the fitted PES at the stationary points, see Fig. 4. Previous results by Sloan *et al.* focused only on the collinear reaction, because they assumed that it was the least energy path.[9] Their approach yielded a $^3\Pi$ collinear transition state with height in the range 0.481–0.537 eV (depending on the basis set used for the *ab initio* calculation) to be compared with our collinear result of 0.291 eV. The assumed linear path led Sloan *et al.*[9] to conclude that a nonadiabatic mechanism (intersystem crossing, ISC, between the singlet $^1A'$ and the triplet $^3A''$ PESs) was necessary to account for the experimental findings. As shown in the panel (a) of Fig. 4, we have obtained a noncollinear saddle point that makes unnecessary the ISC assumption.

The different, almost opposite angular variation of the reactants minimum $M1$ and the saddle point, shown in Fig. 4, implies that the bending motion between these two regions will dramatically determine important features of the reaction dynamics.

Finally, there are no van der Waals minima for configurations corresponding to the collinear approach $\theta=0°$, F···OH and O···FH as shown in the (b) and (c) panels, respectively.

III. WAVE PACKET AND QUASICLASSICAL REACTION DYNAMICS

A. Technical details of the calculations

As QCT calculations regards, with respect to the more standard implementation used in Ref. 10, a modified version of VENUS (Ref. 33) was implemented to comply with the requirements of fixed and constant total angular momentum **J**, derived from our comparing quasiclassical and quantum results. As is in fact well-known[34] since the Hamiltonian is diagonal in J, the quantum number for **J**, its representation is block diagonal in the latter so it is natural to solve the scattering problem for fixed J. Meanwhile, in standard QCT calculations (e.g., in Ref. 10), **J** is varied randomly, normally through random selection of the impact parameter b, in such a way that, after running a large enough batch of trajectories, a good statistics is achieved to enable, for example, a meaningful comparison with experimental data.[35] Instead, for the present application, given J and j of the OH reagent molecule, the initial orbital angular momentum, **l** (where $\mathbf{J}=\mathbf{j}+\mathbf{l}$), for the mutual movement of the F atom and the OH molecule around each other, was appropriately chosen in modulus and orientation. The constancy of **J** was routinely tested in single trajectories and, with the otherwise usual[10] integration conditions (specially, a time step size of 50 as), a conservation of its Cartesian components better than $10^{-5}\hbar$, was achieved.

The wave packet dynamics of $F+OH(v,j)$ reactive collisions was studied using reactant Jacobi coordinates, as described in detail elsewhere:[36,37] **r**, the OH internuclear vector and **R**, the vector joining the OH center-of-mass to the F atom, the angle between them being γ, as illustrated in Fig. 5. A body-fixed frame is used with the three atoms in the x-z plane and the z axis being parallel to the **R** vector. The two radial coordinates, r and R are described in grids, formed by 90×420 equidistant points, in the intervals $0.4\leqslant r\leqslant 5.5$ Å and $0.75\leqslant R\leqslant 13$ Å, respectively. The angle γ is described by 100 Gauss-Legendre quadrature points. Finally, the three Euler angles are described by parity adapted combination of Wigner rotation matrices,[38] characterized by a total angular momentum J and its projections M and Ω on the space-fixed and body-fixed z axes, respectively. The sum over Ω is typi-

TABLE IV. Geometries and energies of the adiabatic stationary points of OHF as calculated from the ground global fit of the $^3A''$ potential energy surface. The (v,n,b) notation corresponds to the harmonic normal modes for OH and HF stretching and OHF bending, respectively. Bond lengths are in Å, angles θ(O-H-F) in degrees, frequencies in cm^{-1} and energies (V) in eV.

	icMRCI+Q	Fitted surface
	Reactant	
r_{OH}	0.9737	0.9735
r_{HF}	...	...
θ	...	...
ω	3723	3723
V	0.000	0.000
V+ZPE	0.230	0.231
	Product	
r_{OH}	...	...
r_{HF}	0.9165	0.9166
θ	...	...
ω	4154	4170
V	−1.443	−1.443
V+ZPE	−1.185	−1.184
	Minimum $M1$	
r_{OH}	0.9822	0.9864
r_{HF}	2.0924	2.1794
θ	66.4	59.7
ω_v	3617	3557
ω_n	344	331
ω_b	575	570
V	−0.230	−0.230
V+ZPE	0.052	0.048
	Minimum $M2$	
r_{OH}	1.9214	1.9177
r_{HF}	0.9308	0.9285
θ	180.0	180.0
ω_v	158	180
ω_n	4031	3750
ω_b	402	341
V	−1.589	−1.587
V+ZPE	−1.279	−1.301
	Transition state	
r_{OH}	1.0330	1.0270
r_{HF}	1.3494	1.3753
θ	109.2	109.6
ω_v	2646	2536
ω_n	1418i	1425i
ω_b	450	336
V	−0.002	0.007
V+ZPE	0.190	0.185

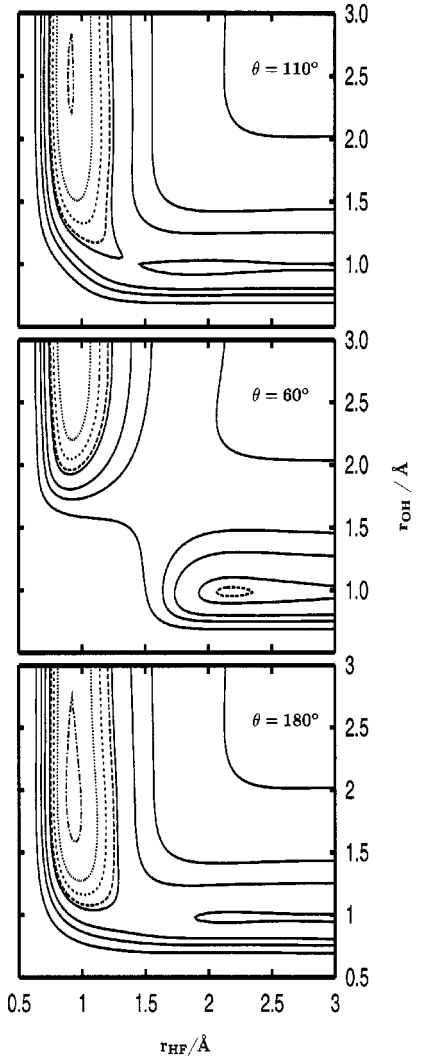

FIG. 3. Contour plots of the fitted $^3A''$ PES for three cuts. Upper panel: bent saddle point (located at an angle θ=109.6°); middle panel: van der Waals reactants well (θ=59.7°); bottom panel; van der Waals products well (θ =180°). The energy contours are −1.5, −1.0, −0.6, −0.2, 0.0, 1.0, 2.0, 4.0 eV, corresponding the solid lines to zero (F+OH asymptote) or positive values.

cally restricted to a single value, the so-called centrifugal sudden approach (CSA), unless otherwise stated.

The integration of the time-dependent Schrödinger equation was performed with a Chebyshev propagator,[39,40] with a time step of 2.5 fs, modified by including absorbing boundary conditions in the polynomial expansion.[41] The damping functions used are $e^{-\alpha(x-x_{abs})^2}$ Gaussian functions, with α=0.01 and 0.035 $Å^{-2}$ and x_{abs}=4 and 11 Å, for r and R, respectively. The time integration is stopped when the reaction probability is converged in the energy interval of interest, typically at times larger than 3–8 ps (depending on J) because of the presence of resonances at low energies. The flux towards products is calculated far from the absorbing region, at r_f=2.5 Å. In order to resolve the narrow resonances appearing at low energies, the flux is analyzed in a dense energy grid, composed of 3001 points in the 0.001–0.75 eV translational energy interval.

The special mass feature of our reaction introduces a noteworthy difficulty in the wave packet propagation which deserves a note of caution. The OH+F→O+HF reaction belongs to the heavy-light+heavy family of reactions, exchanging a light atom between two heavy ones. The PES of such reactions feature, therefore, a rather small skew angle, i.e., a large curvature from reactants to products valleys when mass-weighted and skewed coordinates are used for the representation.[32] This situation introduces also important kinematic restrictions. As an example, the use of reactant Jacobi coordinates to study the products channel presents the inconvenient shown in Fig. 5: because the reactant diatomic center-of-mass is pretty much close to the heavy O atom, the description of HF as the system separates in products re-

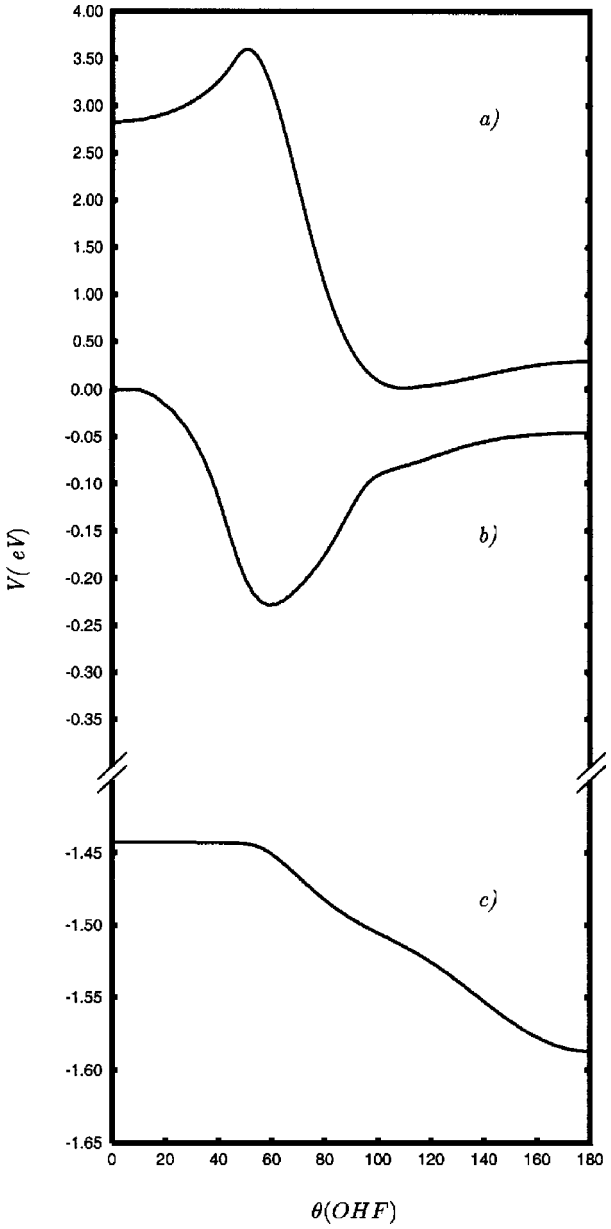

FIG. 4. Angular variation of significant singular points on the PES: Panel (a), barrier height; panel (b), M1 reactant's van der Waals well depth and panel (c): M2 product's van der Waals well depth. Note the change of scale in the energy axis.

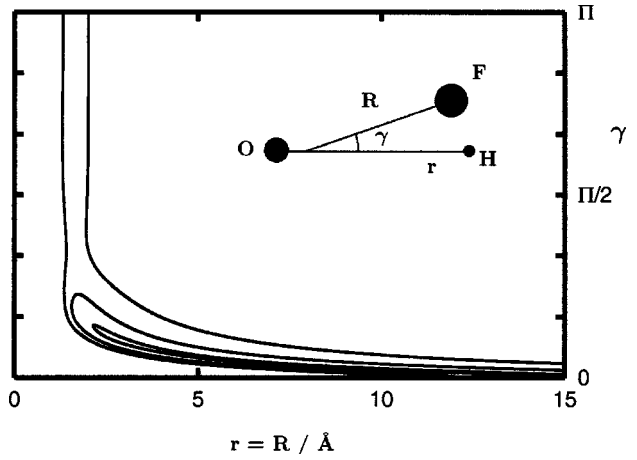

FIG. 5. Contour plots of the potential as a function of $r=R$ and γ. The inset illustrates why $r \approx R$ and $\gamma \rightarrow 0$ to describe the HF products in reactant Jacobi coordinates. The contours correspond to -1.35, 0.5, and 3.75 eV.

quires very long Jacobi vectors, **r** and **R**, of approximately the same length, with the angle between them approaching zero. As a consequence, the number of angular quadrature points necessary to achieve convergence is rather large, 100 in this case. Such large angular grids could be reduced by the use of more adapted coordinates, such as the bond coordinates already applied to the study of Li+HF.[42]

B. Dynamical threshold

The total reaction probabilities as a function of relative translational energy for F+OH ($v=0$, $j=0$, $J=0$) obtained using quantum wave packet and quassiclassical methods are compared in Fig. 6. The overall mutual behavior is in excellent agreement. There is a sort of threshold at ≈ 0.06 eV. This energy corresponds to the $\theta_{\mathrm{OHF}}=180°$ value of the barrier height in Fig. 4(a), opening a wide cone of acceptance below that value down to some 90°. Above this threshold the reaction probability grows rapidly arriving to a maximum at about 0.125 and 0.160 eV, for the quantum and classical methods, respectively. Beyond this maximum the reaction probability decreases nearly monotonically, as expected for exoergic reactions. It does not seem probable that the shift between the maxima of the two methods is due to zero-point energy, because the classical maximum appears at higher energy while, even if we speak of minute values in both cases, the nominal (without ZPE allowance) barrier (7 meV) is higher than the effective (with ZPE) one (-46 meV, as stated above). The region around the maximum between the two wells along the reaction coordinate, in Fig. 2, constitutes the transition state. Such structure appears at $r_{\mathrm{TS}}=1.03$ Å, $R_{\mathrm{TS}}=1.92$ Å, and $\gamma_{\mathrm{TS}}=42°$, as is shown in Fig. 7. The PES looks bound when γ is frozen indicating that this angle acts as a kind of reaction coordinate in Jacobi coordinates, thus playing the role of the HF displacement in bond coordinates $(r_{\mathrm{OH}}, r_{\mathrm{HF}}, \theta)$ as indicated by the imaginary value of the ω_n frequency (see Table IV). The inset of Fig. 5 can help to clarify the point.

Freezing the angle γ at 42°, and solving the resulting Schrödinger equation, a series of bound states are indeed obtained. The lowest of such approximate eigenvalues, 0.178 eV, could be thought of as a sort of ZPE, as confirmed by the good agreement with the harmonic ZPE obtained in Sec. II D. This value is in surprisingly good agreement with the maxima of the classical reaction probability. Two effects could explain why the quantum maximum appears instead at lower energies. One is, of course, the approximated character of this estimation of the transition state zero-point energy, so that the real one is actually shifted towards lower energies. The other reason could be due to the operation of two major reaction mechanisms: one direct, responsible of the threshold, and the second indirect, through resonances near the TS. The classical method would underestimate (or completely miss) the reaction probability at those resonant structures, thus explaining why the quantum probability presents the maximum at lower energies.

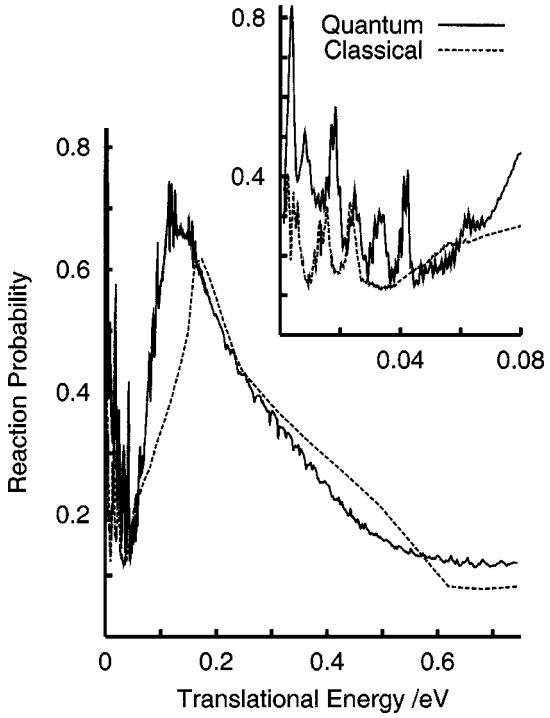

FIG. 6. Total reaction probability for F+OH ($v=0$, $j=0$, $J=0$) obtained using wave packet and quasiclassical methods, as a function of the relative translational energy. The inset shows the detail at very low energy.

C. Transition state resonances associated to periodic orbits

It thus seems that below 0.178 eV the reaction dynamics is mediated by resonances, and it is important to analyze them. Such resonances also appear in recent simulations of the OHF^- photodetachment spectrum performed using the same $^3A''$ PES,[13] to reproduce the experimental data of Bradforth *et al.*[11] These resonances are typical in heavy-light-heavy systems and to better understand their origin an adapted set of coordinates and approximations is convenient. Because O and F atoms are much heavier than the light H atom, it is feasible to adiabatically separate the slow OF vibration from the fast motions associated to the hydrogen atom,[32,43,44] in analogy to the Born-Oppenheimer approximation applied to H_2^+. In Ref. 13 the wave functions associated to these resonances were obtained using a pseudospectral analysis on the wave packet[45–47] and expressed as a function of the $\mathbf{r}_{OF}$ and $\mathbf{R}_{OF—H}$ (with γ' being the angle between these two vectors). The density amplitude plots for large r_{OF} distances (see Fig. 14 of Ref. 13), demonstrate that these resonances correspond to the combination of $HF(v'=3,j')$ and $OH(v=0,j)$ wave functions, with $j'\approx j$. This situation is explained because the $HF(v=3)$ threshold appears at approximately the same energy as $OH(v=0)$, and the rotational constants of the two diatomic fragments are pretty similar. When the two heavy atoms approach each other, the wells appearing in the two rearrangement channels are connected through the saddle point (see Fig. 8). At certain energies, the H atom can fly from one well to the other, thus stabilizing the complex and forming resonances.

A most striking point is that classical results also show a resonant-like structure similar to the one present in the quantum reaction probability. Figure 6 (see especially the inset) shows that below 40 meV collision energy the agreement between the two sets of results is notorious, being the classical peaks shifted towards lower energy values, probably by some zero-point energy effect. At those structures, the classical trajectories become trapped significantly, so that the time propagation should be extended to long times, up to 40 ps, before concluding the trajectory as either reactive or inelastic.

In order to establish a closer connection between the quantum HLH resonances described above and the classical structures, a sort of classical density probability was obtained for classical peaks as follows. About 100 000 trajectories are run at the peak energy and each time they pass within a given

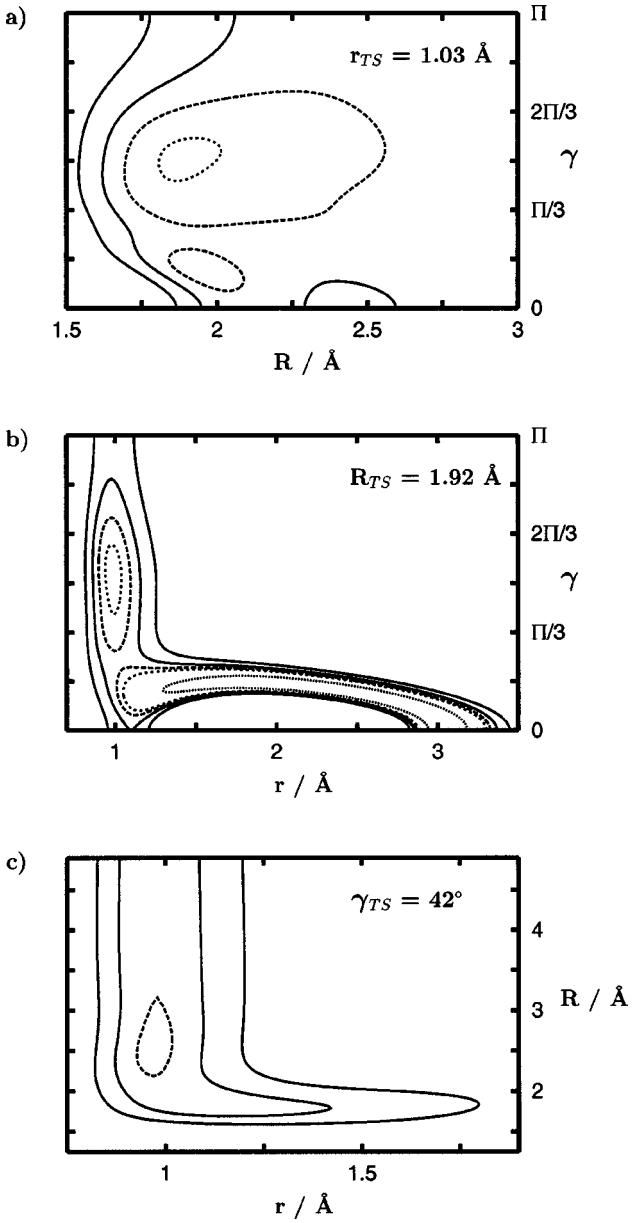

FIG. 7. Contour plots of the PES in the vicinity of the saddle point represented for fixed values of the reactants Jacobi coordinates: (a) $r_{TS}=1.03$ Å, (b) $R_{TS}=1.92$ Å, and (c) $\gamma_{TS}=42°$. The contour energies are -1, -0.4, -0.25, 0, and 0.5 eV referred to the F+OH ($v=0$, $j=0$) asymptote.

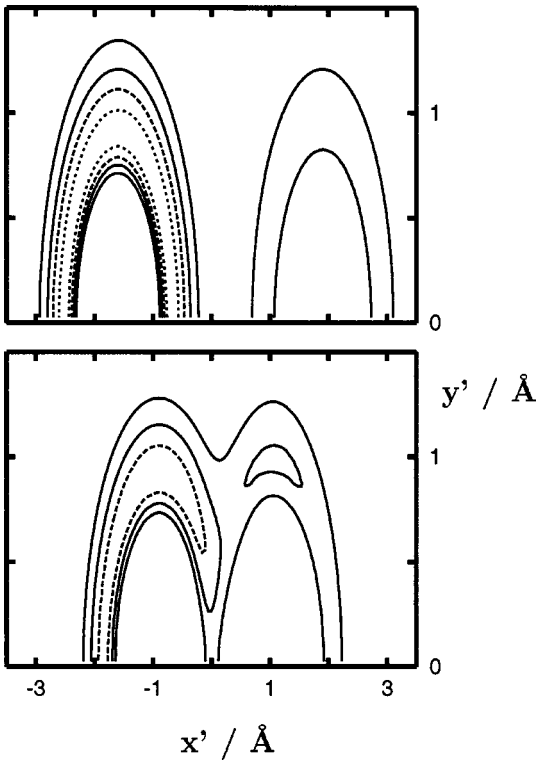

FIG. 8. Contour plots of the OHF($^3A''$) PES as a function of $x' = R_{\text{H-OF}} \cos \gamma'$ and $y' = R_{\text{H-OF}} \sin \gamma'$, in Å, for two different OF distances. Bottom panel: $r_{\text{OF}} = 1.965$ Å, corresponding to the transition state saddle point. Top panel: $r_{\text{OF}} = 3.5$ Å closer to dissociation. The contours are -1.2, -0.5, 0, 1 eV, corresponding the solid lines to zero (F+OH, $v = 0$, asymptote) or positive values.

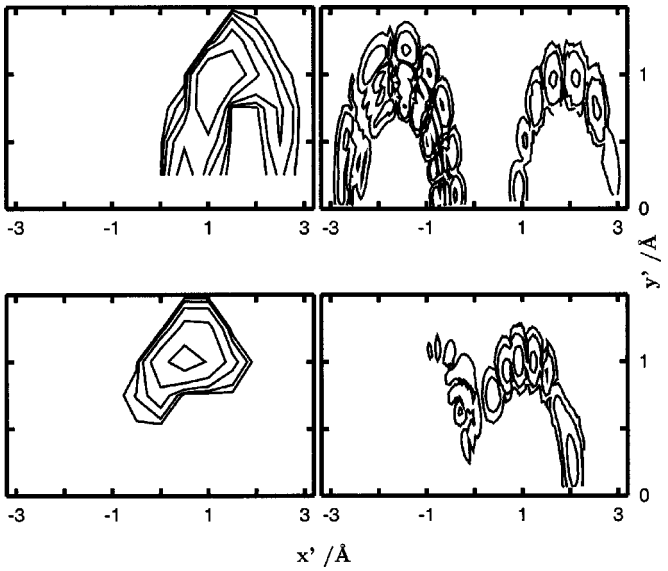

FIG. 9. Quantum/classical amplitude density associated to the HLH resonances/periodic orbits (see text). Bottom, for $r_{\text{FO}} = 1.965$ Å, top for $r_{\text{FO}} = 3.5$ Å. Left, classical results at $E = _{\text{trans}} - 2.5$ meV, right, quantum results for the resonance at $E_{\text{trans}} = 5.0$ meV. The separation between contour lines is 0.1 and 0.2 for the quantum and classical plots, respectively. Also, the classical distribution corresponds to an average over several r_{OF} distances, within a chosen interval, while the quantum distribution corresponds to a single r_{OF} distance.

R_{OF} distance interval they are accumulated in boxes according also to the H-atom position relative to the other two nuclei. As an example, we show in Fig. 9 a classical density probability resultant from 100 000 trajectories for F+OH ($v = 0$, $j = 0$, $J = 0$) at a relative kinetic energy of 2.5 meV, the position of the first classical peak, and compare the results obtained for $R_{\text{OF}} = 1.965$ and 3.5 with quantum results from Ref. 13 obtained for F+OH ($v = 0$, $j = 0$, $J = 0$) and relative kinetic energy of 5.0 meV, the nearest quantum resonance. As the quantum amplitude density, the classical density also shows a maximum in the region of the transition state, although the detailed nodal structure is not present in the classical analog of the HLH resonance amplitude probability. Also, it is difficult to precisely determine low classical density probabilities because it would involve the calculations of an enormous number of trajectories.

In order to better illustrate the kind of trapping involved in these classical resonances, one of those trajectories is shown in Fig. 10. When the two reactants approach each other, the r_{OF} distance decreases down to a minimum value of ≈ 1.8 Å (close to the transition state value), at ≈ 1.5 ps. After this collision the system does not fly apart. Instead, some oscillations in r_{OF} are shown, because the translational energy is transferred towards the OH vibration and/or rotation, thus becoming trapped. A second OF collision occurs at 15 ps, and later the OF oscillation frequency clearly increases. In this situation, the H atom explores the regions of the saddle point ($r_{\text{OF}} = 1.965$ Å, $x' \approx y' \approx 1$ Å, see bottom panel of Fig. 8), as can be seen in panels III–VI of Fig. 10. Suddenly, this trajectory ''finds'' the way towards products as shown in panel VII. There it expends a few oscillations in the well of the products channel and escapes rapidly probably because of the high kinetic energy involved in this channel. A 3D animation of the trajectory fully agrees with this interpretation.

Such ''nearly trapped'' trajectories can be associated to rather stable periodic orbits (PO) at the transition state, responsible for the reaction at these lower energies. Pollak and Child[48] already studied the close connection between these POs and the resonances appearing close to the threshold and called them resonating periodic orbits (RPO). At these RPOs the system oscillates indefinitely from the entrance to the exit channel, what typically requires the presence of wells in both channels. Using the semiclassical method of Gutzwiller,[49] the quantum mechanical resonances are expressed as a sum of POs. In brief, this implies the quantization of the action integrated over the period of one/several POs. Recently, Skodje *et al.*[50] localized the POs associated to the transition state resonances appearing in the F+HD reaction, and conclude that the POs in more than three dimensions become unstable. As an example, some of the resonances appearing in HOCl were interpreted in terms of POs in a bidimensional model.[51] Also, in a study of the photodissociation of Ne-$Br_2(B)$, just below the Ne+Br+Br dissociation threshold, some narrow resonances were found[52] which could be interpreted as a superposition of several POs of horse shoe-type,[53] which nearly coincide with the wave function obtained after spectral quantization of the wave packets. All these studies confirm that the dynamics at the transition state,

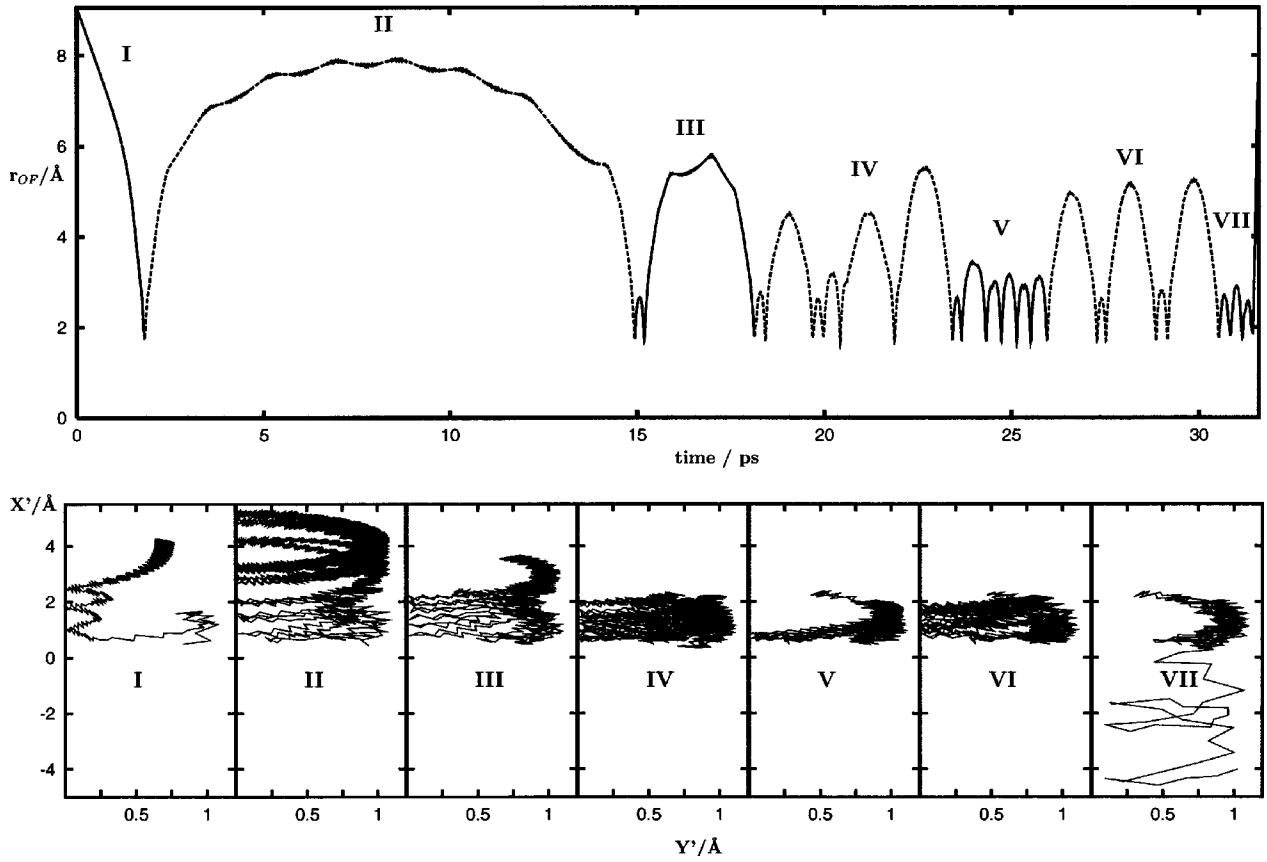

FIG. 10. Top panel: Evolution of the r_{OF} distance as a function of time for a trapped trajectory at $E_{Trans}=2.5$ meV, the most intense "classical peak." This trajectory is divided in seven sectors. For each of them the associated x' and y' values (defined in Fig. 8) along the trajectory are shown in the bottom panels.

either in a collision or a photodissociation process, may be analyzed by semiclassical study of POs.[54]

D. Reaction cross section

It is finally interesting to determine if those resonances persist for higher total angular momenta and if they appear in the reaction cross section. For this purpose, the reaction probabilities for $J=10,20,...,110$ have been calculated using wave packet, within the centrifugal sudden approximation (CSA),[55] as well as quasiclassical methods, and some of the results are compared in Fig. 11. As J increases, the distribution is shifted towards higher energies and the probability decreases, as expected. The narrow structures associated to the HLH resonances described above survive up to quite high J (40 and more), in both quantum and classical results, see Fig. 11. It is interesting to note that the height of the narrow peaks seems to decrease faster in the classical results. Such situation also occurs at $J=0$, for which the wave packet results are "exact" and the classical peaks are lower.

However, in previous calculation on the Li+HF collisions,[36] it was found that the CSA results tend to overestimate the intensity of the peaks of the reaction probability. To check this, a more converged calculation has been performed for $J=40$ including $\Omega=0,1,...,5$, and compared in Fig. 12. The overall reaction probability does not vary significantly, showing the adequacy of the CSA for describing the reaction. For energies above 0.25 eV the agreement is very good. The intensity at the resonances is lower but peaks are broader, similarly to what was found in other reactions.[36] The reason is that all rotational sublevels interact, thus sharing the intensity. Furthermore, the number of accessible dissociative continuum states also increases, and thus their widths also get broader. Since the shift towards lower energy of the quantum maxima was attributed to resonances, the increase of density of states in the exact calculation may explain why the maximum, at 0.2 eV, is higher in the more converged calculations.

The total reaction cross section for F+OH ($v=0$, $j=0$), in Fig. 13, is calculated by adding all partial waves. Classically, this is done by integrating over the impact parameter. In the present CSA treatment, an interpolation is performed to obtain the reaction probabilities for intermediate J's, based on the **J**-shifting approximation.[55] The pure **J**-shifting cross section is not well adapted in this case, because it assumes that the resonant structures persist up to very high **J**'s, thus yielding a significant overestimation of the cross section. The qualitative behavior is, however, acceptable when compared with the CSA and QCT results, which are in rather good agreement. It should be commented that CSA is expected to be rather well converged above 0.1 eV, where the direct mechanism dominates. Below this energy, the indirect mechanism dominates, and the CSA results are expected to overestimate the reaction probability, as discussed above for the case of $\mathbf{J}=40$.

Figure 13 also shows that the cross section is not too sensitive to the resonances, but some more detailed magni-

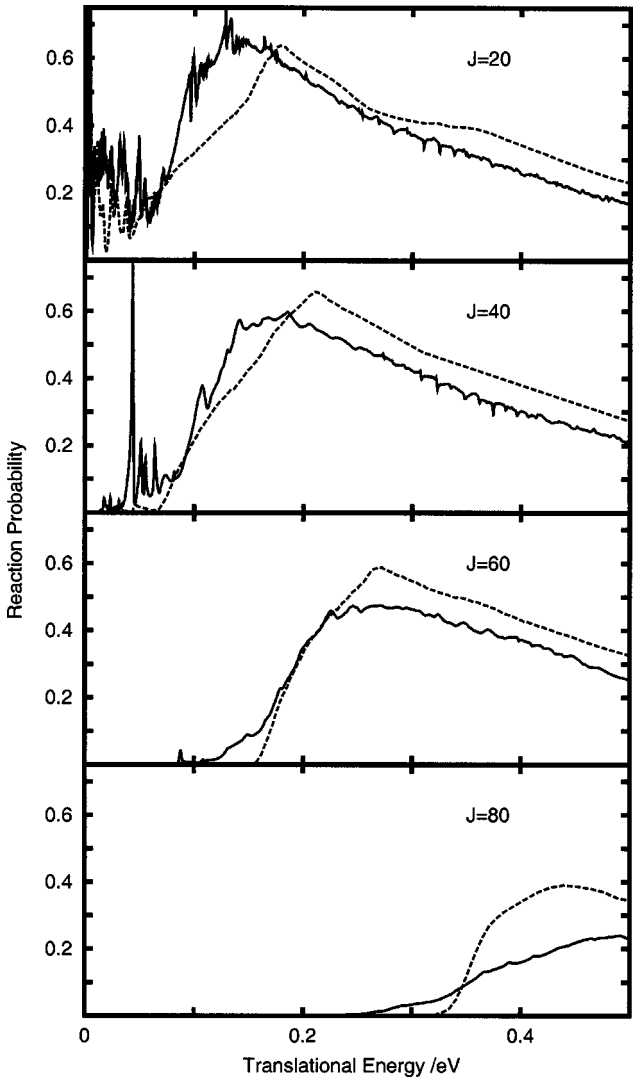

FIG. 11. Quantum CSA (full lines) and quasiclassical (dashed lines) reaction probabilities for F+OH ($v=0$, $j=0$, J).

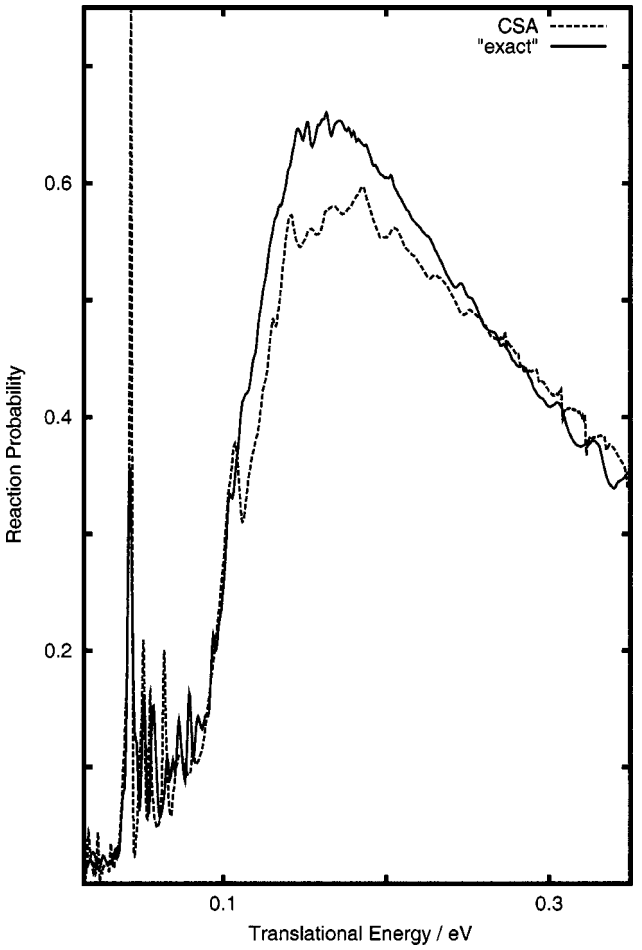

FIG. 12. Comparison between the OH ($v=0,j=0,J=40$)+F reaction probabilities obtained in the CSA (solid line) and "exact" (dashed line) methods, obtained including $\Omega=0$, 1,...,5.

tudes, such as differential cross sections should show clear evidences. Moreover, when these magnitudes are compared with those appearing at higher energies where the reaction follows a direct mechanism, the effect of the HLH resonances should be very evident.

IV. CONCLUSIONS

In this work, highly accurate *ab initio* calculations performed for the OHF system are described for the triplet states corresponding to the ground states of the open shell fragments, $OH(^2\Pi)+F(^2P)$ and $O(^3P)+HF(^1\Sigma^+)$, the OF+H channel being closed at the (thermal) energies of interest. The ground $^3A''$ PES is fitted, with a very small error along the entire minimum energy path. This PES shows that the $OH(^2\Pi)+F(^2P)\rightarrow O(^3P)+HF(^1\Sigma^+)$ reaction is exoergic by some 1.5 eV, with a low, almost negligible barrier, below the zero-point energy of the OH reagents. At both sides of this barrier there are two van der Waals minima, about 0.25 eV deep respect to the appropriate chemical species.

These minima are responsible for the appearance of HLH resonances in the quantum reaction probabilities at low energies. Surprisingly, the QCT results also show peaks in the same energy region, peaks associated to resonating periodic orbits, the classical analog to transition state resonances.

For higher energies, above a threshold of ≈ 0.1 eV, the reaction seems to proceed trough a direct mechanism. This threshold is associated to a "dynamical" zero-point energy at the saddle point. The quantum maximum of the reaction probability is found at lower energies than the classical one, what is explained by the more important role of resonances at these energies.

The relatively high accuracy of the centrifugal sudden approximation is tested for $J=40$, and is used to calculate the reaction cross section. The individual trace of single resonances is washed out in the cross-section variation with translational energy, which, nonetheless, shows a maximum at very low energies due to an indirect reaction mechanism operating through those resonances.

Beyond this maximum the reaction mechanism is direct. In this region, the agreement between CSA and QCT is excellent. The **J**-shifting approach, however, shows a rather bad quantitative behavior because it overestimates the importance of resonances.

Dealing with open shell species, both for reactants and products, more electronic states should actually participate in

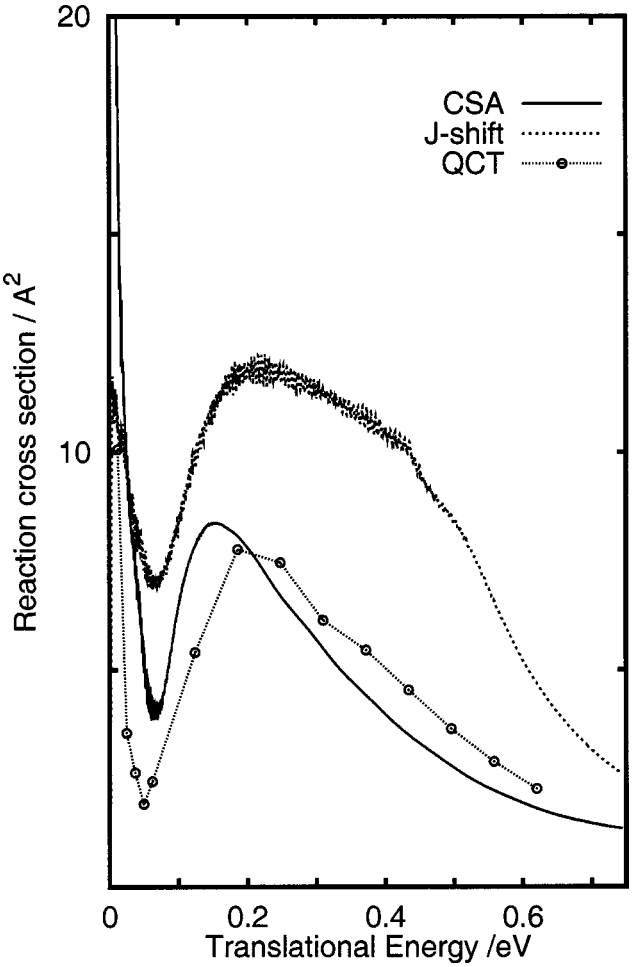

FIG. 13. Total reaction cross section for the F+OH $(v=0,j=0)$ collision, obtained by the CSA, *J* shifting, and quasiclassical methods.

the reaction dynamics. Currently, the fit of the rest of triplets states is being dealt with.[14] Moreover, the nonadiabatic effects are also expected to be rather important and will also being modeled. Finally, also the singlet states, correlating to the excited $O(^1D)+HF(^1\Sigma^+)$ products, could affect the dynamics on triplet states due to spin-orbit couplings.

ACKNOWLEDGMENTS

This work was supported by DGICYT (Ministerio de Ciencia y Tecnología, Spain) under Grants BQU2002-04462-C02-01, BQU2001-0152, and BFM2001-2179. We thank Dr. Aurelio Rodríguez (Universidad del País Vasco, Vitoria) for help with the QCT calculations and the trajectories animation.

[1] R. P. Wayne, *Chemistry of Atmospheres*, 3rd ed. (Oxford University Press, Oxford, 2000).
[2] S. Skokov, T. Tsuchida, S. Nanbu, J. M. Bowman, and S. K. Gray, J. Chem. Phys. **113**, 227 (2000).
[3] T. Martínez, M. L. Hernández, J. M. Alvariño, A. Laganà, F. J. Aoiz, M. Menéndez, and E. Verdasco, Phys. Chem. Chem. Phys. **2**, 589 (2000).
[4] L. J. Butler, Annu. Rev. Phys. Chem. **49**, 125 (1998).
[5] B. Ramachandran and K. A. Peterson, J. Chem. Phys. **119**, 9590 (2003).
[6] B. Ramachandran, E. A. Schrader III, J. Senekowitsch, and R. E. Wyatt, J. Chem. Phys. **111**, 3862 (1999).
[7] T. Xie, D. Wang, J. M. Bowman, and D. E. Manolopoulos, J. Chem. Phys. **116**, 7461 (2002).
[8] C. D. Walther and H. G. Wagner, Ber. Bunsenges. Phys. Chem. **87**, 403 (1983).
[9] J. J. Sloan, D. G. Watson, J. M. Williamson, and J. S. Wright, J. Chem. Phys. **75**, 1190 (1981).
[10] S. Gómez-Carrasco, L. González-Sánchez, A. Aguado, M. Paniagua, O. Roncero, M. L. Hernández, and J. M. Alvariño, Chem. Phys. Lett. **383**, 25 (2004).
[11] S. E. Bradforth, D. W. Arnold, R. B. Metz, A. Weaver, and D. M. Neumark, J. Phys. Chem. **95**, 8066 (1991).
[12] R. N. Dixon and H. Tachikawa, Mol. Phys. **97**, 195 (1999).
[13] L. González-Sánchez, S. Gómez-Carrasco, A. Aguado, M. Paniagua, M. L. Hernández, J. M. Alvariño, and O. Roncero, J. Chem. Phys. **121**, 309 (2004).
[14] L. González-Sánchez, S. Gómez-Carrasco, A. Aguado, M. Paniagua, M. L. Hernández, J. M. Alvariño, and O. Roncero, J. Chem. Phys. (to be published).
[15] S. C. Althorpe and D. C. Clary, Annu. Rev. Phys. Chem. **54**, 493 (2003).
[16] T. H. Dunning, Jr., J. Chem. Phys. **90**, 1007 (1989).
[17] R. A. Kendall, T. H. Dunning, Jr., and R. J. Harrison, J. Chem. Phys. **96**, 6796 (1992).
[18] MOLPRO is a package of *ab initio* programs designed by H.-J. Werner and P. J. Knowles, with contributions from J. Almlöf, R. D. Amos, A. Berning *et al.* (version 2002.7).
[19] H.-J. Werner and P. J. Knowles, J. Chem. Phys. **82**, 5053 (1985).
[20] H.-J. Werner and P. J. Knowles, Chem. Phys. Lett. **115**, 259 (1985).
[21] H.-J. Werner and P. J. Knowles, J. Chem. Phys. **89**, 5803 (1988).
[22] H.-J. Werner and P. J. Knowles, Chem. Phys. Lett. **145**, 514 (1988).
[23] E. R. Davidson, J. Comput. Phys. **17**, 87 (1975).
[24] B. Ramachandran, N. S. Vegesna, and K. A. Peterson, J. Phys. Chem. A **107**, 7938 (2003).
[25] K. A. Peterson, D. E. Woon, and T. H. Dunning, Jr., J. Chem. Phys. **100**, 7410 (1994).
[26] K. P. Huber and G. Herzberg, *Molecular Spectra and Molecular Structure: Constants of Diatomic Molecules* (Van Nostrand Reinhold, New York, 1979).
[27] B. Ruscic, A. F. Wagner, L. B. Harding *et al.*, J. Phys. Chem. A **106**, 2727 (2002).
[28] A. Aguado and M. Paniagua, J. Chem. Phys. **96**, 1265 (1992).
[29] A. Aguado, C. Tablero, and M. Paniagua, Comput. Phys. Commun. **108**, 259 (1998).
[30] D. K. Hoffman, R. S. Nord, and K. Ruedenberg, Theor. Chim. Acta **69**, 265 (1986).
[31] J. Fernández-Rico, A. Aguado, and M. Paniagua, J. Mol. Struct.: THEOCHEM **371**, 85 (1996).
[32] R. D. Levine and R. B. Bernstein, *Molecular Reaction Dynamics and Chemical Reactivity* (Oxford University Press, New York, 1987).
[33] VENUS 96: *A General Dynamics Program, QCPE Program N. 671* (Indiana University, Bloomington, Indiana).
[34] R. T Pack, J. Chem. Phys. **60**, 633 (1974).
[35] D. G. Truhlar and J. T. Muckerman, in *Atom-Molecule Collision Theory: A Guide to the Experimentalist*, edited by R. B. Bernstein (Plenum, New York, 1979).
[36] A. Aguado, M. Paniagua, M. Lara, and O. Roncero, J. Chem. Phys. **107**, 10085 (1997).
[37] M. Lara, A. Aguado, O. Roncero, and M. Paniagua, J. Chem. Phys. **109**, 9391 (1998).
[38] R. N. Zare, *Angular Momentum* (Wiley, New York, 1988).
[39] H. Tal-Ezer and R. Kosloff, J. Chem. Phys. **81**, 3967 (1984).
[40] C. Leforestier, R. H. Bisseling, C. Cerjan *et al.*, J. Comput. Phys. **94**, 59 (1991).
[41] V. A. Mandelshtam and H. S. Taylor, J. Chem. Phys. **103**, 2903 (1995).
[42] M. Lara, A. Aguado, M. Paniagua, and O. Roncero, J. Chem. Phys. **113**, 1781 (2000).
[43] C. Kubach, G. Nguyen, and M. Richard-Viard, J. Chem. Phys. **94**, 1929 (1991).
[44] N. Rougeau, S. Marcotte, and C. Kubach, J. Chem. Phys. **105**, 8653 (1996).
[45] R. Sadeghi and R. T. Skodje, J. Chem. Phys. **102**, 193 (1995).
[46] C. L. Russell and D. E. Manolopoulos, Chem. Phys. Lett. **256**, 465 (1996).
[47] M. Paniagua, A. Aguado, M. Lara, and O. Roncero, J. Chem. Phys. **111**, 6712 (1999).
[48] E. Pollak and M. S. Child, Chem. Phys. **60**, 23 (1981).

[49] M. C. Gutzwiller, J. Math. Phys. **12**, 343 (1971).
[50] R. T. Skodje, D. Skouteris, D. E. Manolopoulos, S.-H. Lee, F. Dong, and K. Liu, J. Chem. Phys. **112**, 4536 (2000).
[51] M. Joyeux, D. Sugny, M. Lombardi, R. Jost, R. Schinke, S. Skokov, and J. M. Bowman, J. Chem. Phys. **113**, 9610 (2000).
[52] O. Roncero, J. Campos-Martínez, M. I. Hernández, G. Delgado-Barrio, P. Villarreal, and J. Rubayo-Soneira, J. Chem. Phys. **115**, 2566 (2001).
[53] R. Prosmiti, P. Villarreal, G. Delgado-Barrio, and O. Roncero, Chem. Phys. Lett. **359**, 229 (2002).
[54] I. Burghardt and P. Gaspard, J. Chem. Phys. **100**, 6395 (1994).
[55] J. M. Bowman, Adv. Chem. Phys. **61**, 115 (1985).
[56] C. E. Miller and B. J. Drouin, J. Mol. Spectrosc. **205**, 312 (2001).
[57] F. Tamassia, J. M. Brown, and Shuji Saito, J. Chem. Phys. **112**, 5523 (2000).
[58] M. W. Chase, J. Phys. Chem. Ref. Data **25**, 551 (1996).